

Self-Driven Hybrid Atomic Spin Oscillator

Erwei Li,^{1,2,†} Qianjin Ma,^{1,2,†} Guobin Liu,^{1,2,*} Peter Yun,^{1,2} and Shougang Zhang^{1,2}

¹*National Time Service Center, Chinese Academy of Sciences, Xi'an, 710600 Shaanxi, China*

²*University of Chinese Academy of Sciences, 100049 Beijing, China*

(Received 1 February 2023; revised 10 May 2023; accepted 16 June 2023; published 14 July 2023)

A self-driven hybrid atomic spin oscillator is demonstrated in theory and experiment with a vapor Rb-Xe dual-spin system. The raw signal of Rb spin oscillation is amplified, phase-shifted, and sent back to drive the Xe spins coherently. By fine-tuning the driving-field strength and phase, a self-sustaining spin-oscillation signal with zero frequency shift is obtained. The effective coherence time is infinitely prolonged beyond the intrinsic coherence time of Xe spins, forming a hybrid atomic spin oscillator. Spectral analysis indicates that a frequency resolution of 13.1 nHz is achieved, increasing the detection sensitivity for a magnetic field. Allan-deviation analysis shows that the spin oscillator can operate in continuous-wave mode like a spin maser. The prototype spin oscillator can be easily incorporated into other hybrid spin systems and can increase the detection sensitivity of alkali-metal–noble-gas comagnetometers.

DOI: 10.1103/PhysRevApplied.20.014029

Alkali-metal–noble-gas comagnetometers have been used for both fundamental and practical applications, such as the search for axionlike particles or new physics beyond the standard model [1–4] and inertial-navigation gyroscopes [5–7]. It is important for the comagnetometer detection sensitivity for a magnetic field or angular velocity to be continuously increased to beat the frequency or energy limits of record-breaking measurements [3,8,9].

Basically, comagnetometer sensitivity is determined by two main factors: the coherence time and the signal-to-noise ratio (SNR) of the spin-oscillation signal. To increase the SNR, various parametric modulations together with lock-in detection are regularly used to suppress the noise [3,9–11]. Signals can be amplified with use of a smart optical design such as multipass vapor cells [12,13]. For the coherence time, increasing the spin longitudinal relaxation time is the first consideration. Buffer-gas filling [14] and antirelaxation paraffin coating [15] in vacuum atomic vapor cells have been used in atomic clocks and magnetometers for a long time, so the techniques have been inherited naturally for alkali-metal–noble-gas comagnetometers. Multiple spatial or temporal spin-field interactions, such as separated oscillating fields (producing the Ramsey fringe in atomic fountain clocks) [16] and Hahn-echo or spin-echo and Carr-Purcell-Meiboom-Gill pulse-excitation techniques in nuclear-magnetic-resonance (NMR) spectroscopy [17–19], can also effectively increase

the transverse relaxation time or coherence time of spin oscillations.

Inspired by the self-oscillating nonlinear-magneto-optical-rotation magnetometer of Schwindt *et al.* [20], we have long wondered whether a self-sustaining spin oscillator based on an alkali-metal–noble-gas comagnetometer is possible. Compared with magnetometers using only alkali-metal atoms, alkali-metal–noble-gas comagnetometers have the advantage of a much-longer nuclear spin relaxation time, typically from tens of seconds to even hours, for example, with ³He [21], and the nuclear spin coherence can be transferred to alkali-atom spin in the hybrid spin dynamics [22]. It is thus theoretically easier for such a system to become self-oscillating given proper feedback conditions. Here we propose a self-driven hybrid atomic spin oscillator theoretically and demonstrate its feasibility by a simple-to-establish experimental apparatus.

We consider a model Rb-Xe comagnetometer in self-feedback or self-driving mode, where the driven spin dynamics can be described by the coupled Bloch equations

$$\begin{aligned} \frac{\partial \mathbf{M}^{\text{Rb}}}{\partial t} &= \frac{\gamma_{\text{Rb}}}{q} \mathbf{M}^{\text{Rb}} \times (\mathbf{B}_0 + \lambda \mathbf{M}^{\text{Xe}}) + \frac{M_0^{\text{Rb}} \hat{z} - \mathbf{M}^{\text{Rb}}}{q T^{\text{Rb}}}, \\ \frac{\partial \mathbf{M}^{\text{Xe}}}{\partial t} &= \gamma_{\text{Xe}} \mathbf{M}^{\text{Xe}} \times (\mathbf{B}_0 + \lambda \mathbf{M}^{\text{Rb}} + G M_x^{\text{Rb}} e^{i\theta} \hat{y}) \\ &\quad + \frac{M_0^{\text{Xe}} \hat{z} - \mathbf{M}^{\text{Xe}}}{T^{\text{Xe}}}. \end{aligned} \quad (1)$$

where \mathbf{M}^{Rb} and \mathbf{M}^{Xe} are the Rb and Xe spin magnetizations, respectively, $M_0^{\text{Rb}} \hat{z}$ and $M_0^{\text{Xe}} \hat{z}$ are the initial Rb and Xe spin magnetizations in the z direction, respectively, \mathbf{B}_0 is the static magnetic field, T^{Rb} and T^{Xe} are the Rb and Xe

*Corresponding author. liuguobin@ntsc.ac.cn

†E. Li and Q. Ma contributed equally to this work and are joint first authors.

spin relaxation times, respectively, q is the slowing-down factor due to Rb-Xe spin-exchange collisions at high temperature, $\lambda = 8\pi\kappa/3$ ($\kappa \sim 500$ for Rb-Xe spin-exchange interaction) is the enhancement factor due to Fermi-contact interaction between Rb valence electrons and Xe nuclei [22], and γ_{Rb} and γ_{Xe} are the gyromagnetic ratios for Rb and Xe spins, respectively. The undefined parameters and the numerical solving procedure are described in our previous work [23].

The driving term $GM_x^{\text{Rb}} e^{i\theta} \hat{y}$ is the phase-shifted spin oscillation of Rb spins in the transverse direction, and it couples with Xe spins transversely like a conventional NMR excitation-pulse protocol. In this case, the equivalent spin dynamics of the comagnetometer is as follows: first, the fast-relaxing Rb spins adiabatically follow the slowly precessing Xe spins under the overdamping condition as in classical driven oscillators [24]; secondly, the Rb spin-oscillation signal is amplified, phase-shifted, and sent back to drive the Xe spins as an ac magnetic field. Thus, the hybrid spin system forms a self-driven oscillator. For experimental realization, the Rb spins also act as a probe, reading out the Xe spin-precession signal. The driving-field strength is determined by the gain factor G , and the driving field is in phase or out of phase depending on the phase shift θ .

The comagnetometer works in two modes: open-loop mode ($G = 0$) and closed-loop mode ($G \neq 0$). In closed-loop mode, the self-driving comagnetometer can work in two different states depending on the magnitude of G . In classical oscillator electronics, a closed-loop system can be made self-oscillating when the product of the gain and feedback approaches 1. By simulation, we found a similar critical condition for the closed-loop comagnetometer to become self-oscillating, which in this case is described as

$$GM_0^{\text{Rb}} \sim \lambda M_0^{\text{Xe}} / q, \quad (2)$$

meaning the self-oscillating behavior can be triggered when the driving-field strength approaches $(1/q)$ th of the initial Xe spin magnetization. It is key to note that the signal amplitude of the comagnetometer output in the open loop is proportional to the Rb spin-magnetization strength, while the long-time oscillation behavior is governed by the Xe spin precession. This makes Eq. (2) have the present form. The driving mechanism can be understood as a variation of the conventional π -pulse Hahn-echo sequence [17]. The excitation or driving field is an always-near-resonant wave with moderate strength, rather than a short, strong, and broadband radio-frequency pulse. As the driving field circulates continuously in the closed-loop mode, multiple echos can occur and persist for different times depending on G . When the driving field reaches a threshold strength such that the amplitude of the echos ceases decreasing, the spin oscillation reaches a steady state.

However, we have to point out that Eq. (2) is an empirical relation as concluded by numerical-simulation results. There are probably other factors, such as the intrinsic coherence time of nuclear spins T_2^{Xe} , playing a certain role in the driving mechanism. However, we cannot change T_2^{Xe} much once the experimental setup is constructed, so here we take T_2^{Xe} as a fixed parameter (approximately 10 s). For typical experimental conditions, the initial Rb and Xe spin magnetizations are at the same level, i.e., $\lambda M_0^{\text{Rb}} \sim \lambda M_0^{\text{Xe}} \sim 0.1 \text{ mG}$ [1]. So for the $^{87}\text{Rb}-^{129}\text{Xe}$ spin pairs, the threshold driving-field strength obtained by simulation is given by $G_{\text{sim}} M_0^{\text{Rb}} \sim \lambda M_0^{\text{Xe}} / q \sim 20 \mu\text{G}$, i.e., $G_{\text{sim}} \sim 1000$.

Generally, the self-driving-field strength can be divided into two regions: (1) when $GM_0^{\text{Rb}} \leq \lambda M_0^{\text{Xe}} / q$, the self-driving field is said to be weak since the Xe spin oscillation decays exponentially as usual; (2) when $GM_0^{\text{Rb}} \geq \lambda M_0^{\text{Xe}} / q$, the self-driving effect becomes strong and a self-sustaining spin oscillation emerges, with an effective coherence time far longer than the intrinsic spin relaxation time of ^{129}Xe spins in typical temperature and buffer-gas conditions, as shown by the two insets in Fig. 1.

The phase is also critically important in realization of the self-sustaining spin oscillation. Simulation results show that the self-sustaining oscillation can persist for a phase range determined by

$$\theta_0 < \theta < 180^\circ - \theta_0, \quad (3)$$

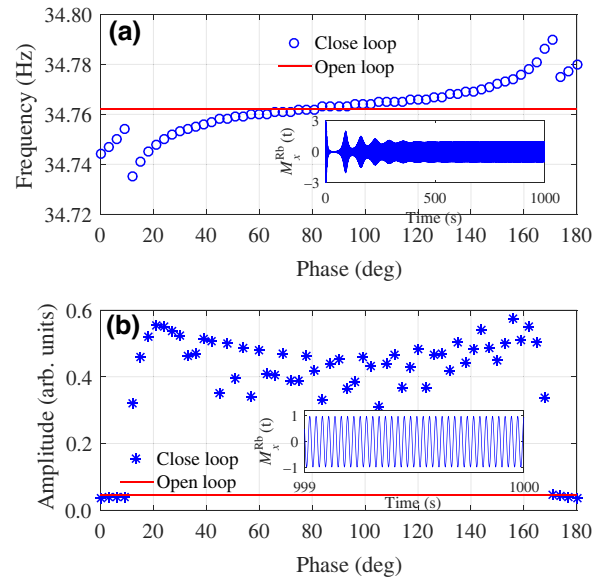


FIG. 1. Simulated self-driving spin-oscillation signal (a) in closed-loop mode and (b) its frequency response as a function of the self-driving phase shift θ at a fixed strong gain $G = 1000$. The crossing between the open-loop curve (red line) and the closed-loop curve (blue circles) indicated there is a phase point where ZFS occurs despite the presence of the Bloch-Siegert-shift effect under a strong off-resonance self-driving field.

as indicated by the two sharp structures in the frequency-phase (dispersions) and amplitude-phase (steps) diagrams in Fig. 1. The greater is G , the smaller is θ_0 , meaning a wider phase range for self-sustaining oscillation exists given a stronger self-driving field.

It is also shown in Fig. 1(b) that the frequency shifts almost linearly with θ in most of the self-sustaining-oscillation phase range given by Eq. (3) except at around the critical phase points at θ_0 and $180^\circ - \theta_0$. The shift can be explained as follows: due to the Bloch-Siegert-shift effect in NMR spectra [25], the mismatch of the initial phase values between the driving-field signal and open-loop signal can lead to an accumulation effect, which may keep changing gradually the closed-loop frequency. In this case, one may think the self-driven comagnetometer is not suitable for precision measurements despite the potential advantages in signal amplification and lengthening of the coherence time.

However, by numerically solving Eq. (1), we find a phase point where the spin-oscillation frequency shift vanishes. As shown in Fig. 1(a), the frequency of the closed loop (blue circles) crosses that of the open loop (red line), implying that the frequency shift vanishes at a certain phase value. Theoretically the in-phase driving phase value is 90° considering the y -axis-excitation and x -axis-detection configuration; however, due to the Bloch-Siegert-shift effect, the zero-frequency-shift (ZFS) phase θ_{ZFS} is about several degrees below 90° . The position of θ_{ZFS} depends also on G . The larger is G , the further is θ_{ZFS} from 90° . The existence of the ZFS phase is important as we have to rule out any possible nonsystematic-frequency-shift sources [8] to find out the fundamentally unknown spin-dependent interactions.

To verify the simulation results, we construct a Rb-Xe comagnetometer setup and specially design the driving electronics with tunable gain and phase parameters, as depicted in Fig. 2.

The main part is a typical Rb-Xe comagnetometer, with a vacuum atomic vapor cell containing a Rb-Xe gas mixture at high temperature (approximately 120°C) as the atom-spin medium. The cell is spherical with a diameter of about 10 mm, containing 4-Torr ^{129}Xe and 35-Torr ^{131}Xe and several tens of torr of N_2 as a buffer gas. The cell is placed in the center of three sets of Helmholtz coils orthogonal to each other. The three sets of coils have current-to-magnetic-field conversion coefficient $C_{B-I} \sim 1-2 \text{ mG/mA}$. For the B_y coil, it is 2 mG/mA. The driving current can be changed by fine-tuning a rheostat (from 1 to 100 k Ω) in series with the coil. A circularly polarized 795-nm laser with power of approximately 54 mW in the z direction shines into the cell to align the Rb-atom spins. Then the Rb spin polarization is transferred to Xe-atom spins via rapid spin-exchange collisions [26]. The polarized Xe spins drive Rb spins in a classical way [24], and finally a linearly polarized 780-nm laser with power of approximately 3

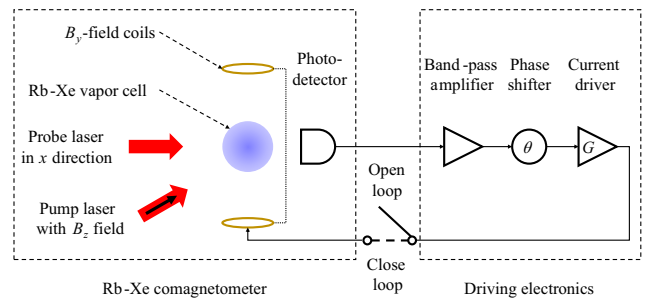


FIG. 2. Experimental schematic of the self-driving Rb-Xe spin oscillator. It consists of a typical pump-probe Rb-Xe comagnetometer (left) and driving electronics with tunable gain and phase parameters (right). The pump-laser and probe-laser powers are 54 and 3 mW, respectively. The static field B_z is approximately 30 mG, corresponding to a ^{129}Xe spin-oscillation frequency $v_0 \sim 35 \text{ Hz}$.

mW in the x direction reads out the Rb spin dynamics over time as the comagnetometer original output signal. Here, for simplicity, we use a single symbol for the photodetector, while it actually includes a high-extinction-ratio linear polarizer and a polarized beam splitter forming a high-sensitivity optical-polarimeter detection scheme [10].

The driving electronics are basically a combination of a band-pass amplifier, a phase shifter, and a current driver. The center frequency of the band-pass filter is 35 Hz, with a Q factor of 10, meaning a passing-band frequency range of approximately $35 \pm 1.75 \text{ Hz}$. Thus, the ^{131}Xe spin-oscillation signal at approximately 10 Hz is suppressed in the closed-loop mode. Two factors affect the design of the driving electronics. First, the Rb spins have a larger response than Xe spins at lower frequency. Secondly, for typical applications including magnetic field and rotation-rate measurements, Rb-Xe comagnetometers usually work in an ultralow-frequency range. Both factors require the target spin oscillation to be working in the range from several hertz to a few tens of hertz. Unfortunately, the $1/f$ law of noise spectra indicates the spin-oscillation signal may be easily disturbed by loud amplitude and phase noises in the frequency range. While the gain G has high tuning resolution, the phase resolution $\Delta\theta$ is limited to a few degrees.

For one typical experimental cycle, we first break the link between the Rb-Xe comagnetometer and the driving electronics and record an open-loop spin-oscillation signal, as shown in Fig. 3(a). Then we restore the link, set the electronics driving output to a fixed gain, and change the phase point by point with an accuracy of a few degrees, recording the spin-oscillation signals accordingly. Finally, we fix the phase to the ZFS point, where the closed-loop spin-oscillation frequency coincides with the open-loop one, and record a long-time spin-oscillation signal, as shown in Fig. 3(b).

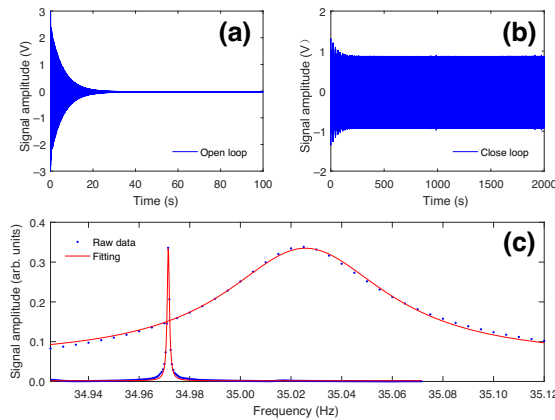


FIG. 3. Spin-oscillation signals of the self-driving Rb-Xe spin oscillator in (a) open-loop mode and (b) closed-loop mode, and (c) comparison of the corresponding Fourier spectra. A linewidth narrowing by a factor of 75 and an SNR increase by a factor of 34 are achieved when we switch from the open-loop mode to the closed-loop mode. The open-loop Fourier spectra in (c) are magnified by 10 times to increase visibility.

It is experimentally found that the self-oscillation is triggered when the driving current of the B_y coil reaches approximately 20 μA , i.e., driving-field strength $B_y \sim 40 \mu\text{G}$. By measuring the frequency shift of Xe spin precession $\Delta\nu_{\text{Xe}}$ while reversing the pump-laser polarization from σ^+ to σ^- , we determine the Rb spin magnetization field experienced by Xe spins to be $\Delta\nu_{\text{Xe}}/\gamma^{\text{Xe}} = 0.1 \text{ Hz}/(11.78 \text{ MHz/T}) = 0.085 \text{ mG}$ in our system, so the Rb spin magnetization field in a vacuum is $0.085/\lambda \sim 0.02 \mu\text{G}$. Therefore, the experimental threshold gain factor $G_{\text{exp}} = B_y/M_0^{\text{Rb}} \sim 2000$. This threshold driving-field strength is about 2 times larger than the simulated values. Considering the uncertainty in the estimated values of M_0^{Rb} and M_0^{Xe} and other parameters (such as κ and T_2^{Xe}), the experimental results agree well with the simulation results within the allowed error range.

With standard Fourier analysis and a standard data-fitting process, we extract the spin-oscillation frequency versus phase and find it agrees with the simulation results in Fig. 1(b). As shown in Fig. 3(c), a spectral linewidth of 0.04 Hz with SNR of approximately 1200 and a spectral linewidth of 0.53 mHz with SNR of approximately 40 600 are obtained for the open-loop and closed-loop signals, respectively. Compared with the open-loop operation, the frequency resolution of the ^{129}Xe spin resonance frequency is increased by a factor of approximately 2540, from 33.3 μHz to 13.1 nHz, approaching state-of-the-art accuracy [3]. For ^{129}Xe with gyromagnetic ratio of 11.78 MHz/T, this level of frequency resolution leads to a magnetic field resolution of approximately 1.11 fT, which is sufficient for applications such as the detection of the human-brain magnetic field [27]. The noise-equivalent magnetic field power spectral density is given in Fig. 4,

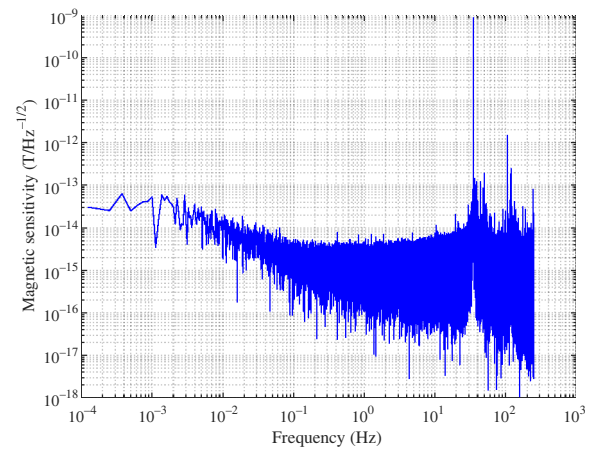


FIG. 4. Sensitivity of the Rb-Xe comagnetometer measured as the power spectral density of the noise-equivalent magnetic field. The magnetic field sensitivity reaches $10 \text{ fT}/\text{Hz}^{1/2}$ or less in a frequency range from 0.01 to 10 Hz. Note the spike at approximately 35 Hz is the ^{129}Xe spin resonance peak.

showing a magnetic sensitivity of $10 \text{ fT}/\text{Hz}^{1/2}$ or less achieved in the frequency range from 0.01 to 10 Hz, which is helpful for various applications from biomagnetism detection to fundamental physical instrumentation.

It should be noted that the center frequencies of closed-loop and open-loop signals do not coincide exactly with each other due to the limited tuning resolution of phase control by rheostats in the present experiment. This could be easily improved with higher-phase-tuning techniques, such as a direct digital synthesis.

We observe the spin-oscillation signal with a real-time oscilloscope for hours and find no sign of decay at all, which means that the effective coherence time of spin oscillation is probably infinite. Once the loop is open, the spin oscillation starts to decay exponentially again within the intrinsic coherence time of noble-gas spin. In this sense, the self-driving comagnetometer can be taken as a hybrid atomic spin oscillator, preferably working in continuous-wave mode like a conventional laser or maser.

To test the performance of the hybrid spin oscillator in long-term operation, we record continuously the spin oscillation for 10 000 s in the closed-loop mode and perform a standard Allan-deviation analysis for the last 9000 s, as shown in Fig. 5. The frequency instability of spin oscillation reaches 2.99 μHz at an averaging time of 2048 s, which is equivalent to a bias instability of approximately 3.87°/h for gyroscopic measurement.

With respect to the 13.1-nHz frequency resolution, the 2.99- μHz frequency instability is relatively high. We attribute this deterioration to various frequency-drift sources. For example, we observe for 2 days a correlation between the drift of the spin-oscillation frequency (at the 10^{-4} level) and the drift of the heater power for a vapor

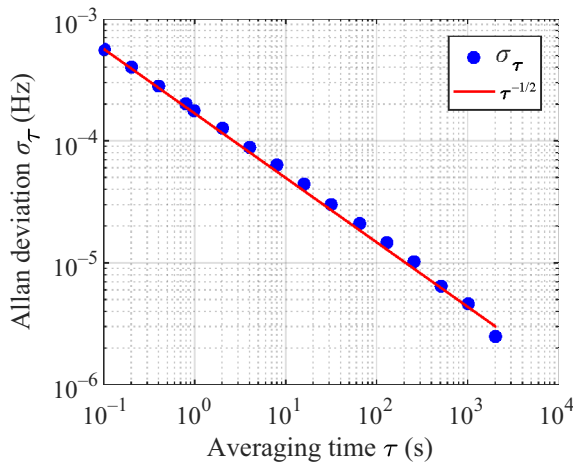


FIG. 5. Allan deviation of the ^{129}Xe spin-oscillation frequency for averaging time up to 2048 s. A frequency instability of $2.99 \mu\text{Hz}$ is achieved at a measuring time of 2048 s, which is equivalent to a bias instability of $3.87^\circ/\text{h}$.

cell, which is a result of the slowly varying residual magnetic field produced by the leaky current of the heater wires. Besides, the pump-laser power is in free-running mode, whose fluctuation can cause significant fluctuation (at the 1% level) of the optical pumping rate, and thus the fluctuation of alkali atomic spin magnetization, which finally causes the frequency shift of the noble-gas spin oscillation. There are other factors affecting the medium-term to long-term frequency instability, such as the drift of current feeding the bias-field coils.

As indicated in Fig. 1(a), the fluctuation of the unlocked phase can also lead to a frequency shift with a slope of $\delta\nu/\delta\theta \sim 10^{-4} \text{ Hz per degree}$. A possible improvement is to use the phase-locking method [28] to lock the driving phase at the ZFS point. Considering the infinite effective coherence time, the self-driving spin oscillator has the potential to reach a frequency instability at the nanohertz level with long-term running. As shown in Fig. 4, σ_τ continues going down at 2048 s, indicating a better frequency stability can be reached given a longer running time.

During the preparation of the manuscript, we noticed the work of Jiang *et al.* [29], which presented similar phenomena. We emphasize the following important differences between their work and ours. First, we build the spin oscillator with a simpler prototype setup, neither an external driving field nor parametric modulation (together with lock-in detection) is used in the experiment and no significant SNR loss is observed. Secondly, we derive the self-oscillating conditions for the Rb-Xe comagnetometer by developing a different theoretical framework, especially the introduction of G and θ , which are conceptually convenient for understanding and easier to use for guiding the experiment. Finally, we find

the existence of zero-frequency-shift phase in theory and experiment, which is important for various applications in precision measurement physics.

Compared with the ^3He and ^{129}Xe Zeeman masers reported by Chupp *et al.* [30], the most-important differences between their scheme and our scheme are the detection methods. We have Rb spins and Xe spins in a single vapor cell, with Rb spins as the probe for Xe spin-precession signals. We also use an optical polarimeter for reading out the spin-precession signal, instead of the traditional pick-up coils based on Faraday electromagnetic induction [30]. Both arrangements increase the detection sensitivity theoretically. However, the single-cell scheme does not allow us to optimize the pump and probe parameters separately, which could be done with the separate pump cell and probe cell scheme in Ref. [30]. The single-cell arrangement is also disadvantageous due to the back-action of Rb spin magnetization on the Xe spin precession in the detection period. Besides, we use single-nuclear-spin species instead of two-nuclear-spin species. This results in our scheme having greater sensitivity to the magnetic field drift. Both arrangements can worsen the long-term frequency stability in our scheme.

Compared with the colocated ^{129}Xe and ^{131}Xe spin masers of Sato *et al.* [31], the major difference is their introduction of ^{131}Xe spins in addition to ^{129}Xe spins. This scheme can theoretically decrease the systematic frequency errors due to the magnetic field fluctuation; however, the nonzero nuclear quadrupole moment of ^{131}Xe can render the system sensitive to stray electric fields, worsening the long-term frequency stability. Besides, they used a transmission detection on the probe laser, which could cause more noise compared with the polarimeter detection in our scheme. Costly photoelastic modulation and lock-in detection was also used to increase the signal-to-noise ratio in Ref. [31], while our scheme does not use any external modulation or lock-in detection and still reaches the same level of signal output of approximately 1 V.

Generally, the demonstrated self-driven hybrid atomic spin oscillator is still in its preliminary stage, needing further optimization in some areas, including the magnetic field drift control and laser-power stabilization. However, it has already shown great potential in precision measurement with a simple-to-establish setup. In principle, the demonstrated spin-oscillator scheme can also be applied to other dual-spin systems, such as the K- ^3He comagnetometer, and also to trispin comagnetometers, such as the Rb- ^3He - ^{129}Xe or Rb- ^{129}Xe - ^{131}Xe configuration [3,13] with careful design of dual-channel driving electronics with respect to the two noble-gas spin-oscillation frequencies.

In conclusion, we demonstrate theoretically and experimentally a self-driving spin oscillator based on the Rb-Xe comagnetometer. A self-sustaining oscillator with infinite coherence time is realized under proper driving conditions. The spin-oscillation frequency shift vanishes at

certain phase points despite the Bloch-Siegert-shift effect. The frequency resolution of the hybrid spin oscillator reaches the level of approximately 10 nHz, potentially increasing the detection sensitivity for magnetic or gyroscopic measurements with a simple apparatus. The magnetic sensitivity reaches a level of $10 \text{ fT/Hz}^{1/2}$ or less in the frequency range from 0.01 to 10 Hz, which is very useful for various applications from biomagnetism detection to fundamental physical instrumentation. With further improvement with regard to frequency instability, the hybrid atomic spin oscillator could work like a laser or maser for long-time operation, which is promising for various scientific or practical applications, such as search for new spin-dependent interactions and Earth-rotation monitoring.

ACKNOWLEDGMENTS

G.L. thanks Dong Sheng and Min Jiang from the University of Science and Technology of China for helpful discussions. The authors also appreciate the financial support of the Chinese Academy of Sciences under Grant No. E209YC1101 and of the National Time Service Center under Grant No. E024DK1S01.

- [1] M. Bulatowicz, R. Griffith, M. Larsen, J. Mirijanian, C. B. Fu, E. Smith, W. M. Snow, H. Yan, and T. G. Walker, Laboratory Search for a Long-Range T -Odd, P -Odd Interaction from Axionlike Particles Using Dual-Species Nuclear Magnetic Resonance with Polarized ^{129}Xe and ^{131}Xe Gas, *Phys. Rev. Lett.* **111**, 102001 (2013).
- [2] M. Pospelov, S. Pustelny, M. P. Ledbetter, D. F. Jackson Kimball, W. Gawlik, and D. Budker, Detecting Domain Walls of Axionlike Models Using Terrestrial Experiments, *Phys. Rev. Lett.* **110**, 021803 (2013).
- [3] M. E. Limes, D. Sheng, and M. V. Romalis, ^3He - ^{129}Xe Comagnetometry Using ^{87}Rb Detection and Decoupling, *Phys. Rev. Lett.* **120**, 033401 (2018).
- [4] N. Sachdeva *et al.*, New Limit on the Permanent Electric Dipole Moment of ^{129}Xe Using ^3He Comagnetometry and SQUID Detection, *Phys. Rev. Lett.* **123**, 143003 (2019).
- [5] E. A. Donley, Nuclear magnetic resonance gyroscopes, *2010 IEEE Sensors*, 17 (2010).
- [6] T. W. Kornack, R. K. Ghosh, and M. V. Romalis, Nuclear Spin Gyroscope Based on an Atomic Comagnetometer, *Phys. Rev. Lett.* **95**, 230801 (2005).
- [7] T. G. Walker and M. S. Larsen, Spin-exchange-pumped NMR gyros, *Adv. At. Mol. Opt. Phys.* **65**, 373 (2016).
- [8] W. A. Terrano, J. Meinel, N. Sachdeva, T. E. Chupp, S. Degenkolb, P. Fierlinger, F. Kuchler, and J. T. Singh, Frequency shifts in noble-gas comagnetometers, *Phys. Rev. A* **100**, 012502 (2019).
- [9] A. Almasi, J. Lee, H. Winarto, M. Smiciklas, and M. V. Romalis, New Limits on Anomalous Spin-Spin Interactions, *Phys. Rev. Lett.* **125**, 201802 (2020).
- [10] D. Budker, W. Gawlik, D. F. Kimball, S. M. Rochester, V. V. Yashchuk, and A. Weis, Resonant nonlinear magneto-optical effects in atoms, *Rev. Mod. Phys.* **74**, 1153 (2002).
- [11] D. A. Thrasher, S. S. Sorensen, J. Weber, M. Bulatowicz, A. Korver, M. Larsen, and T. G. Walker, Continuous comagnetometry using transversely polarized Xe isotopes, *Phys. Rev. A* **100**, 061403(R) (2019).
- [12] S. Li, P. Vachaspati, D. Sheng, N. Dural, and M. V. Romalis, Optical rotation in excess of 100 rad generated by Rb vapor in a multipass cell, *Phys. Rev. A* **84**, 061403(R) (2011).
- [13] C.-P. Hao, Q.-Q. Yu, C.-Q. Yuan, S.-Q. Liu, and D. Sheng, Herriott-cavity-assisted closed-loop Xe isotope comagnetometer, *Phys. Rev. A* **103**, 053523 (2021).
- [14] H. G. Dehmelt, Slow spin relaxation of optically polarized sodium atoms, *Phys. Rev.* **105**, 1487 (1957).
- [15] M. A. Bouchiat and J. Brossel, Relaxation of optically pumped Rb atoms on paraffin-coated walls, *Phys. Rev.* **147**, 41 (1966).
- [16] N. F. Ramsey, A new molecular beam resonance method, *Phys. Rev.* **76**, 996 (1949).
- [17] E. L. Hahn, Spin echoes, *Phys. Rev.* **80**, 580 (1950).
- [18] S. Meiboom and D. Gill, Modified spin-echo method for measuring nuclear relaxation times, *Rev. Sci. Instrum.* **29**, 688 (1958).
- [19] M. H. Levitt, *Spin Dynamics: Basics of Nuclear Magnetic Resonance* (Wiley, Chichester, UK, 2001).
- [20] P. D. D. Schwindt, L. Hollberg, and J. Kitching, Self-oscillating rubidium magnetometer using nonlinear magneto-optical rotation, *Rev. Sci. Instrum.* **76**, 126103 (2005).
- [21] T. R. Gentile, P. J. Nacher, B. Saam, and T. G. Walker, Optically polarized ^3He , *Rev. Mod. Phys.* **89**, 045004 (2017).
- [22] T. W. Kornack and M. V. Romalis, Dynamics of Two Overlapping Spin Ensembles Interacting by Spin Exchange, *Phys. Rev. Lett.* **89**, 253002 (2002).
- [23] G. Liu, Trispin dynamics in an alkali-metal–noble-gas nuclear-magnetic-resonance gyroscope, *Phys. Rev. A* **99**, 033409 (2019).
- [24] G. Liu, V. Guarnera, S. Gu, and S. Zhang, Response dynamics of an alkali-metal–noble-gas hybrid trispin system, *Phys. Rev. A* **104**, 032827 (2021).
- [25] F. Bloch and A. Siegert, Magnetic resonance for nonrotating fields, *Phys. Rev.* **57**, 522 (1940).
- [26] T. G. Walker and W. Happer, Spin-exchange optical pumping of noble-gas nuclei, *Rev. Mod. Phys.* **69**, 629 (1997).
- [27] H. Xia, A. Ben-Amar Baranga, D. Hoffman, and M. V. Romalis, Magnetoencephalography with an atomic magnetometer, *Appl. Phys. Lett.* **89**, 211104 (2006).
- [28] K. Zhang, N. Zhao, and Y. H. Wang, Closed-loop nuclear magnetic resonance gyroscope based on Rb - Xe , *Sci. Rep.* **10**, 2258 (2020).
- [29] M. Jiang, H. Su, Z. Wu, X. Peng, and D. Budker, Floquet maser, *Sci. Adv.* **7**, eabe0719 (2021).
- [30] T. E. Chupp, R. J. Hoare, R. L. Walsworth, and B. Wu, Spin-Exchange-Pumped ^3He and ^{129}Xe Zeeman masers, *Phys. Rev. Lett.* **72**, 2363 (1994).
- [31] T. Sato *et al.*, Development of co-located ^{129}Xe and ^{131}Xe nuclear spin masers with external feedback scheme, *Phys. Lett. A* **382**, 588 (2018).